TECHNISCHE MECHANIK
an open access journal

journal homepage: www.ovgu.de/techmech

Tech. Mech., Vol. 43, Is. 1, (2023), 38–48

Received: 27.01.2023
Accepted: 08.02.2023
Available online: 16.02.2023

Use of High-Order Curved Elements for Direct and Large Eddy Simulation of Flow over Rough Surfaces

Kenan Cengiz*, Sebastian Kurth, Lars Wein, and Joerg R. Seume

Leibniz Universität Hannover, Institute of Turbomachinery and Fluid Dynamics. An der Universität 1, DE-30823 Garbsen

Abstract: In the present study, the curved element capabilities of a high-order solver are scrutinized for use in scale-resolving simulations regarding roughness. The approach devised not only suggests a plausible way to adopt a body-fitted grid approach as an alternative to immersed boundary method (IBM), but also enables performing LES instead of DNS without under-resolving the roughness. The method is first tested using various polynomial degrees. Then, it is validated against reference DNS-IBM results from a rough channel flow setup having various Reynolds numbers corresponding to the entire roughness range. The results confirm the validity of the new approach. Finally, a highly loaded low-pressure turbine cascade is simulated under LES resolution with and without the roughness patch. Although a rougher surface is needed for producing a more pronounced impact on the flow, the viability of this method also for pressure-gradient boundary layers is proven.

Keywords: curved elements, DNS, high-order discretization, ILES, roughness

1 Introduction

The Direct Numerical Simulation (DNS) of the flow over rough surfaces has been a hot topic amongst the fluid research community, because understanding the influence thereof on the flow can be significant in industrial applications. For instance, deciding when to replace turbomachinery blades to retain the roughness-related performance degradation at acceptable levels requires a reliable prediction of the influence.

Roughness increases losses in the flow due to higher production of turbulence: higher turbulence due to a change in momentum transfer between fluid and surface leads to thickening of the boundary layer, and to higher losses. On top of this, other properties of the blade such as the location of separation bubbles or the transition point are affected by the change of the boundary layer flow (Roberts and Yaras, 2005).

DNS provides a good amount of information for building, and tuning roughness models in Reynolds-averaged Navier-Stokes (RANS) approaches. The current trend to perform DNS of flow over roughness persists in the immersed-boundary method (IBM) for a reason. In fact, IBM is definitely superior to the classical body-fitted grid approach when complex roughness is in question, making it effortless to cover realistic rough surfaces with perfect mesh quality (Leonardi et al., 2007; Chung et al., 2021). However, one is often restricted to DNS because the resolution of the roughness becomes essential in addition to the resolution of the flow, particularly in the range from hydraulically smooth to transitionally rough regimes. On top of that, there can be a need for a DNS with very high resolution of turbulence to fully represent the roughness sufficiently, resulting in fairly high computational costs for such low Reynolds numbers (Thakkar et al., 2018).

The impact of a simplistic artificial roughness on the flow over a low-pressure turbine (LPT) blade is investigated by Joo et al. (2016) using a large-eddy simulation (LES) approach on body-fitted structured grids. Even though the findings are quite interesting, the regularly distributed box-like roughness elements don't represent a real rough surface. Another remarkable example to the eddy-resolving simulation of flow over a uniform regular roughness could be the work by Vadlamani et al. (2018), where a high-order finite difference scheme is used for thorough investigation of the transition to turbulence due to the roughness.

The IBM approach is adopted in many investigations of roughness (Leonardi et al., 2007; Busse et al., 2015; Thakkar et al., 2017; Hartung et al., 2018; Kurth et al., 2021). They are mainly based on rigorous simulations in channel flows to scrutinize the effects of different roughness characteristics such that useful roughness correlations and models can be deduced for use in RANS of industrial applications. Simulating roughness on real applications, such as turbomachinery blades, is a relatively new research area. Only recently have the computationally demanding resources required become fairly affordable. Such resources are not only needed for adequate resolution of the flow, but also for resolution of the roughness elements over the blade. In a recent study, Hammer et al. (2018) experimented with two approaches to incorporating the roughness effect into the flow over a T106A cascade in their LES simulations: 1) adding a source term to the governing equations to serve as a roughness model, 2) applying the "boundary data immersion method", akin to IBM, to an as-cast surface on the same blade. The latter case requires that they go up to a DNS-level resolution on the rough surface, so that the effect of smaller roughness elements are not missed. The former approach, on the other hand, despite being cost-effective, proved to be a mere approximation to the impact of roughness.

In the present study, the possibility to curve the high-order elements is exploited for high-fidelity flow simulation over rough surfaces. To the authors' knowledge, this is a rather novel approach. The closest study that was found is by Garai et al. (2018);

* E-mail address: cengiz@tfd.uni-hannover.de
doi: 10.24352/UB.OVGU-2023-043

Denison et al. (2019). They used a space-time discontinuous Galerkin spectral-element method applied on artificial roughness, which is generated as sinusoidal displacement of the surface using a linear-elasticity analogy (Diosady and Murman, 2018). On the other hand, real roughness is considered in the present work. A discontinuous Galerkin scheme based on flux reconstruction (FR) is used, wherein the mesh is fitted to the roughness using arbitrary inverse-distance weighted smoothing (Karman et al., 2016). The study is done in two steps: 1. A filtered roughness is examined only, where fitting the faces of the polynomial-based elements on the roughness should not be troublesome. 2. A low-pressure turbine (LPT) cascade having an unfiltered roughness is analyzed.

2 Simulation Setup

2.1 Methodology and the Numerical Solver

A high-order solver called PyFR (version 1.12.2) is utilized. The numerical scheme is based on flux reconstruction with the DG correction function, where polynomial degrees up to $p = 4$ for mixed elements are possible. The solver is designed not only for DNS, but also for implicit large-eddy simulation (ILES), where the abruptly increasing numerical dissipation is used as the surrogate subgrid model. A detailed description of the solver is given in Witherden et al. (2014).
On the element interfaces, a Rusanov Riemann solver is applied. A Local Discontinuous Galerkin Scheme (LDG) scheme, with the upwind and penalty parameters of $\beta = 0.5$ and $\tau = 0.1$, is used for the viscous fluxes. The time marching is based on the explicit RK45[2R+] scheme with proportional-integral (PI) adaptive time-step controlling. The Gauss-Legendre flux and solution point sets are used. Unless stated otherwise, anti-aliasing through approximate L^2 projection of flux in the volume and on the face using 9th-order quadrature is activated. This is indeed considered necessary because aliasing-driven instabilities can become severe in the case of highly curved elements. Another reason is the spurious transfer of energy from the unresolved modes to the resolved ones, which can be even higher in under-resolved configurations (such as ILES) without using anti-aliasing.
The simulations are conducted with single-precision number representation. In fact, adequacy of the single precision was shown by Witherden and Jameson (2020) for similar scale-resolving simulations.
In the present investigation, not only the flow solver's support for curving elements, but also the support of the mesh generation software is vital. In other words, if the mesh generation software lacks the support of high-order elements, the flux points placed on the face of the resulting linear element would not improve the representation of the rough surface at all.

2.2 The Rough Surface for Validation and the Mesh Parameters

Since validation of the proposed method is targeted initially, the IBM-DNS results by Thakkar et al. (2018) over the surface "s8" are considered, where a wide range of roughness heights (as well as Reynolds numbers) are covered. The surface was extracted from measurements of a grit-blasted surface. The surface's aerodynamically irrelevant smaller scales (Mejia-Alvarez and Christensen, 2010) were eliminated with a low-pass filter. The details of the data acquisition and filtering procedure are explained by Busse et al. (2015). In order to keep Re_τ high enough while lowering roughness levels (from $k^+ = 30$ to 3.75), the roughness patch was first scaled down by 2, 4 and 8, then tiled accordingly (as in Table 1). The same conditions as the reference benchmark are adopted for the validation, except that the computational domain is a half channel with a symmetry condition on the mid-plane.
For a computational domain with flat boundaries, elevating the order of the linear elements would be as simple as adding planar nodes on the faces and in the volume. Nevertheless, adding planar nodes on the faces would not be a good representation of curved geometries. Hence, the face nodes must be placed on the boundary defined by the given geometry. For example, this is made possible through defining subdividing the surface mesh and finding the interpolation polynomial over them Krais et al. (2021). The resulting high-order mesh must also be smoothed because the curved boundary may result in inverted elements, especially in the tightly packed boundary layer regions Krais et al. (2021). The readers interested in the mesh curving methods can refer to the review by (Hindenlang et al., 2015). In the present study, curving of the elements is handled during the export of the mesh using Pointwise (Karman et al., 2016). This involves three stages:

1. Elevate the linear elements to high-order elements by adding new interior and face nodes. Fictional linear sub-elements are formed in the process.
2. Perturb the nodes using a perturbation field based on inverse distance weighted smoothing
3. Improve the mesh quality by applying an optimization-based smoothing on the linear sub-elements. The resulting sets of linear sub-elements form the high-order elements of high quality.

Polynomial degrees up to $Q = 4$ are possible in the mesh export process. In order to adequately fit the perceived surface (i.e. the resulting mesh boundary) to the original surface (i.e. the geometry model), a mesh export with $Q \geq 2$ as well as simulations with $p \geq 2$ is desired. The selection of high Q values during the mesh export may initially sound plausible to ensure a good representation of the original surface. However, the mesh export process can easily get troublesome because of convergence difficulties during the smoothing phase. Since the original surface in question is filtered, $Q = 2$ is found to be sufficient.
A qualitative comparison of the surfaces provided by $Q = 1$ and $Q = 2$ is shown in Figure 1. Clearly, the $Q = 2$ mesh better represents the original CAD geometry. Note that the visualization tool uses the uniform nodes provided by the mesh and utilizes Lagrange polynomials to interpolate. From the perspective of the flow solver, however, there is no guarantee for the surface flux points to be located on the original geometry because the point sets used by the mesh generation tool and the flow solver are different. After reading the uniformly distributed points given by the mesh generator, the flow solver creates its own points (Gauss-Legendre) on the projected surface based on the provided points.
Table 1 gives details about the simulations as well as the mesh. The same mesh is used for all simulations, but with different p.

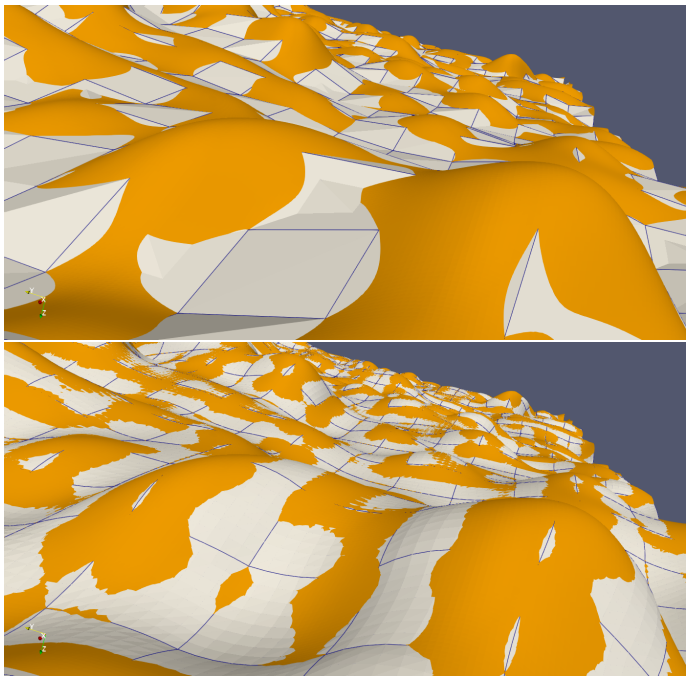

Fig. 1: A view from the wall boundary. top: $Q = 1$ (with $p = 1$); bottom: $Q = 2$ (with $p = 4$). The orange surface is the original CAD geometry. The gray surface represents how the surface is interpreted by the flow solver.

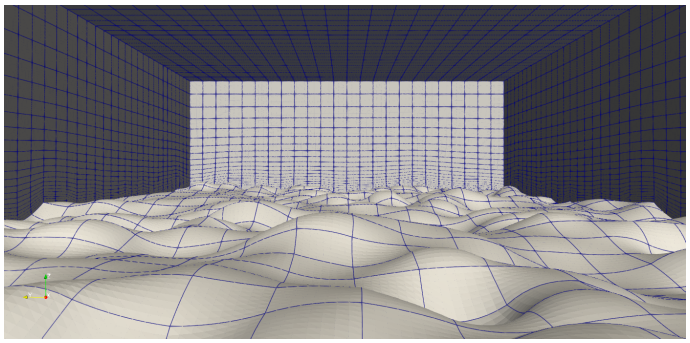

Fig. 2: The computational domain and the surface mesh ($Q = 2$).

The mesh consists of $48 \times 24 \times 22$ elements in streamwise, spanwise, and wall-normal directions, respectively. The height of the first element is taken to be $z^+ \approx 1.76$ for $\mathrm{Re}_\tau = 180$, corresponding to $z^+ \approx 7.04$ for the $\mathrm{Re}_\tau = 720$ case. Therefore, the first Gauss-Legendre solution point (denoted as $z^+_{\mathrm{eff.}}$) falls well below $z^+ = 1$ for all simulations. The computational boundaries and the wall surface mesh can be seen in Figure 2, where the curvature of the wall boundary can also be observed clearly. The view direction of the snapshot is the streamwise ($+x$) direction; the left boundary is in the $+y$ direction; and the top boundary is the channel mid-plane ($z = \delta$), on which the symmetry condition is enforced. All lateral boundaries are subject to periodic conditions in the respective directions.

The down-scaled patches (Simulations 1–3 in Table 1) may require higher polynomial degrees ($Q > 2$) for the same mesh because the topology can feature multiple extrema in one direction in one element. Therefore, $Q = 3$ is chosen for the surfaces with lower roughness (Simulations 1–2).

For an accurate simulation, adequate representation of the roughness by the mesh is crucial. For the evaluation of accuracy, some roughness parameters are used. The mean roughness height Sa, the maximum roughness height Sz, the skewness SSk, and the effective slope ESx in main flow direction are calculated according to DIN EN ISO 25178-2 (DIN EN ISO 25178-2, 2012). The equivalent sand-grain roughness ks is calculated with the ks-correlation of Sigal and Danberg (1990) using the shape and density parameter by Dirling (1973). Figure 3 shows the relative differences of these roughness parameters calculated for the representation by the higher order mesh ($Q = 2$) and a linear mesh ($Q = 1$) in comparison to the roughness parameters of the original surface geometry. It can be seen that the representation of the roughness by the linear mesh decreases all roughness parameters. The highest relative difference is found for the equivalent sand-grain roughness (-0.29). The representation of the roughness by a higher-order mesh significantly improves the fidelity. The highest difference, once again found for the equivalent sand-grain roughness, is reduced to -0.03. All in all, the higher-order mesh provides a satisfactory representation of the original surface topology.

Tab. 1: The conducted simulations over the surface s8. Number of elements ($N_x \times N_y \times N_z$) is $48 \times 24 \times 22$ for all of the simulations. No anti-aliasing is used for 4c.

simulation #	k^+	Re_τ	tiles	$\Delta x^+, \Delta y^+$	$\Delta x^+_{\mathrm{eff.}}, \Delta y^+_{\mathrm{eff.}}$	$z^+_{\mathrm{eff.}}$	Q	p	precision
1	3.75	180	8×8	21.2	5.3	0.13	3	3	SP
2	7.5	180	4×4	21.2	5.3	0.13	3	3	SP
3	15	180	2×2	21.2	5.3	0.13	2	3	SP
4a	30	180	1×1	21.2	4.2	0.08	2	4	DP
4b	30	180	1×1	21.2	7.1	0.20	2	2	SP
4c	30	180	1×1	21.2	5.3	0.13	2	3	SP
4d	30	180	1×1	21.2	5.3	0.13	2	3	SP
4e	30	180	1×1	21.2	5.3	0.13	1	3	SP
5	60	360	1×1	42.3	10.6	0.25	2	3	SP
6	90	540	1×1	63.5	12.7	0.25	2	4	SP
7	120	720	1×1	84.6	17.0	0.34	2	4	SP

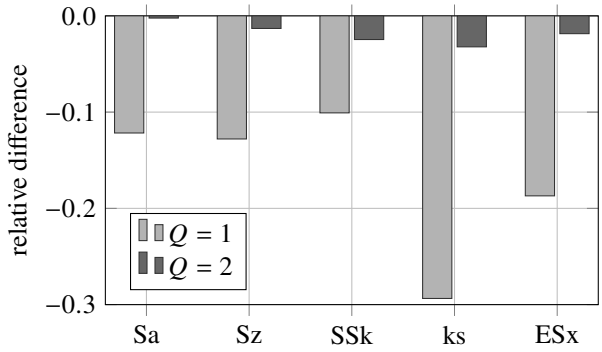

Fig. 3: Comparing differences of roughness parameters calculated for the roughness represented by the higher order mesh ($Q = 2$) and a linear mesh ($Q = 1$) (in Table 1 simulations 4a and 4e) relative to the roughness parameter of the input surface.

3 Results

3.1 Validation on Rough Channel

A plain channel flow with periodic conditions in streamwise (x) and spanwise (y) directions are considered. In fact, such an arrangement is a substantially efficient way to investigate the effect of roughness on the boundary layers. The compressible Navier-Stokes equations for an ideal gas with constant viscosity are solved. No turbulence model is in question, leading to either a DNS or an Implicit Large Eddy Simulation (ILES) depending on the resolution and the polynomial degree. The Mach number is kept below 0.2 for all cases.

A set of simulations are conducted in the channel to investigate several numerical effects as well as the effect of Reynolds number. Table 1 lists the simulations with their roughness height, Reynolds number, and the resolutions they provide. The effective resolutions give an idea about the resolving power of the high-order method based on the number of freedom degrees in the element. Moreover, z^+_{eff} takes the approximate location of the first solution point over the surface. It can be deduced that the high Reynolds number cases ($Re_\tau = 360, 540, 720$) correspond to an ILES, whereas the lower Re_τ cases are of DNS resolution.

The simulations start from stillness, where the flow is driven by a constant body force in the x-direction, ensuring the nominal Re_τ values in Table 1). After an initial transient phase of at least $60\delta/u_\tau$, the flow statistics are collected for around $80\delta/u_\tau$. This is found to be sufficient according to Figure 4, where the sampling error is estimated based on the mean-square error (MSE) of the sample mean $\overline{g}$,

$$\mathrm{MSE}\,(\overline{g}) = \frac{\mathrm{Var}_N(g)}{N} \tag{1}$$

according to Bergmann et al. (2021). Here, $\mathrm{Var}_N(g) = \frac{1}{N}\sum_{i=0}^{N-1}(g_i - \overline{g})^2$ is the biased estimate of the population variance. It is observed that the estimated sampling error agrees with the nominal Re_τ value, which is imposed as a body force. The reason the nominal value cannot be precisely reached may be uncertainties relating to the force integration, the compressibility, and the sampling error altogether.

Before presenting results from the entire range of roughness, some validation tests on $\mathrm{Re}_\tau = 180$ are conducted (simulations 4a–e in Table 1). The results are gathered in Figure 5. Firstly, the highest resolution is considered (Simulation 4a). It achieves a DNS resolution with $240 \times 120 \times 110$ degrees of freedom in streamwise, spanwise, and normal directions, respectively (cf. Thakkar et al. (2018)). At the same time, DP is used, as commonly required by a proper DNS. Compared to Simulation 4d, using of $p = 4$ and DP together does not improve the mean velocity profile discernibly, although the turbulence quantities get closer to the reference IBM-DNS. It should be noted that the quantities deviate from the reference towards the channel mid-plane because the half-channel simplification is adopted, unlike in the reference setup. The lowest possible polynomial approximation ($p = 2$), which

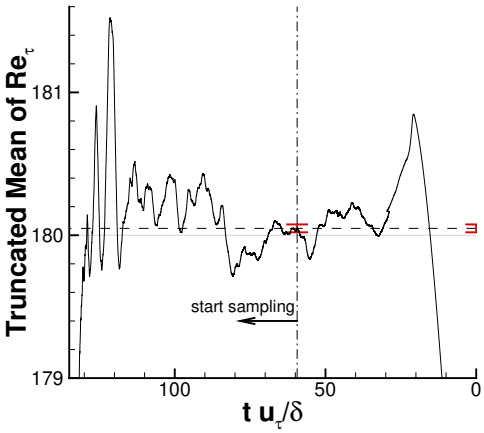

Fig. 4: Truncated mean of effective Re_τ calculated from the force on the wall for Sim. 4d (Tab. 1). *Dashed:* the mean; *Gray:* the nominal value $Re_\tau = 180$; *Red:* error bar for the mean

can sufficiently imitate the surface topology ($Q = 2$) as shown in Figure 3, is also considered (Sim. 4b). Once again, while the mean velocity profile is of acceptable accuracy, there is a clear over-prediction in the turbulence kinetic energy. Another interesting test is the effect of anti-aliasing (Sim. 4c). Even though the simulation does not crash due to the aliasing-related instabilities, the accuracy is impaired. Thus, anti-aliasing is used for all of the simulations. Lastly, the effect of low-order surface approximation is tested (Sim. 4e). A linear approximation to the roughness ($Q = 1$), as seen in Figure 1 degrades the velocity profile prediction and the prediction of the turbulent quantities. On the other hand, a higher degree of approximation to the surface improves the results considerably.

The streamwise mean velocity profiles for the entire range of roughness are shown in Figure 6. There is a good agreement with the reference DNS for all cases. Particularly for the highest Reynolds number ($\mathrm{Re}_\tau = 720$), the simulation falls into an ILES. Even so, the impact of the roughness (i.e. roughness function ΔU^+) seems to be predicted accurately. The mean velocity profile prediction over the tiled surface also agrees with the reference DNS. However, there is a slight mismatch for the two lowest roughnesses. The reason is that the polynomials no longer fit the original geometry well, even though the polynomial degree of the mesh export is raised to $Q = 3$. Although a better fit could be ensured by refining the mesh, even without a refinement, the coverage of the roughness peaks and valleys is obviously far better compared to an IBM approach with the same resolution. This is because an IBM perception of one $k^+ = 3.75$ high roughness element could yield a complete disregard of the roughness element. Consequently, further refinement of the grid was found to be necessary for the reference IBM-DNS to be able to resolve the roughness. In fact, Thakkar et al. (2018) had to use $\Delta x^+ = \Delta y^+ = 0.44$ for the $k^+ = 3.75$ case, which would correspond to an over-resolution of the flow in the smooth case. The computational cost savings by the present approach in such a setting are obviously immense. For instance in Simulation 2, the number of degrees of freedom used in the present study and the reference IBM-DNS are 1.622 millions and 63.7 millions for the half-channel, respectively. In settings where $k^+ \geq 15$ however, the possible costs saved should be of the level achieved when one moves from DNS to LES, assuming that the same solver and the hardware is used.

Figure 7 is a snapshot showing the isosurface of Q-criterion coloured by the velocity magnitude for the case with the highest Reynolds number. It illustrates how flow structures smaller than the mesh element can be captured without sacrificing the curvature of the boundary. For the same simulation, the resolved turbulence on a spanwise plane can be viewed in Figure 8.

3.2 T106C Low-Pressure Turbine Cascade

T106C low-pressure turbine cascade has been a benchmark test for validating flow solvers. It is a highly loaded blade with a pitch-to-chord ratio of 0.95. Each blade measures $c = 93.01$ mm in chord length and $c_{\mathrm{ax}} = 79.9$ mm in axial chord length. The inlet flow angle is 32.7°. The original experiment covers Reynolds numbers ranging from 80,000 to 250,000 with an inflow turbulence intensity of 0.9%, 1.8%, and 3.2% (Michálek et al., 2012). The outlet Mach number is fixed at $M = 0.65$. In the present investigation, Re = 80,000 with 0.9% turbulence intensity is considered, which was also the choice by *the 2nd Workshop on High-Order CFD*. The inlet air temperature is taken as $T_i = 298.15$ K. The ratio of the specific heat is fixed at $\gamma = 1.4$, and the specific gas constant is $R = 287.1\ \mathrm{J \cdot kg^{-1} \cdot K^{-1}}$. On the blade, a no-slip adiabatic wall condition is imposed. A fixed total pressure of $p_{0,\mathrm{inlet}} = 7198.5$ Pa is enforced at the inlet, whereas Riemann-invariant conditions with a static pressure of 5419.3 Pa are set. More details about the setup can be found in the workshop's web page (DLR, 2013).

Figure 9 shows the computational domain for the smooth mesh. The rough mesh is actually identical except for the refined block on the roughness patch (Figure 10a). The mesh is extruded in the spanwise direction for a length of $0.2c$, being divided in 21 elements. The elements are elevated to $Q = 3$ for fitting the roughness as much as possible, whereas $Q = 2$ was found to be sufficient for the smooth blade. In total, the rough and smooth cases consist of 180,726 and 173,082 elements, respectively. Both simulations are run with a polynomial degree of $p = 3$.

The simulation is initially run for a simulation time of around $158c/U_{\mathrm{out}}$ to wash away the transients, then for $167c/U_{\mathrm{out}}$ to collect the statistics. According to Bergmann et al. (2021), this proved to be a sufficient amount of time with acceptable sampling error.

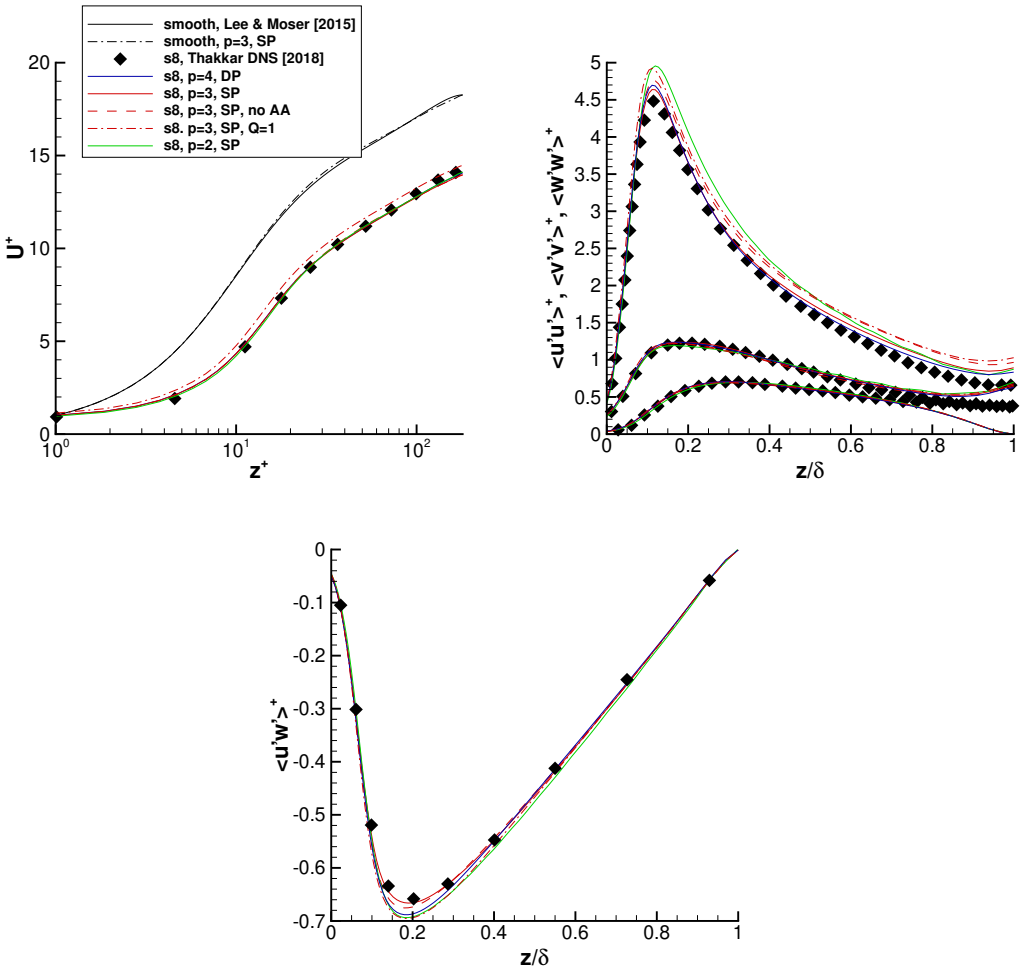

Fig. 5: Mean velocity profiles (top left) and turbulence variances (top right, bottom) in wall units for $\mathrm{Re}_\tau = 180$. Black symbols represent IBM-DNS by Thakkar et al. (2018)

On top of that, spatial averaging in the spanwise direction is also adopted for further improvement.
Figure 11 compares the original rough surface to the roughness perceived by the solver. The roughness patch is blended into the smooth blade using a linear function, leaving no abrupt change on the border of the patch. Clearly, some detail of the roughness is lost due to the discretization because a real roughness is essentially C0 continuous only. That is, the roughness cannot easily fit C1 continuous polynomials. Although a better representation of a filtered roughness–such as "s8" in the previous section–would be possible, we choose not to filter the surface because the discretization itself already behaves like a filtering process based on piecewise polynomials.
The resolution in wall units is demonstrated in Figure 10b for the rough blade. Evidently, the curves with dense wiggles represent the distributions on the rough suction side. The $\Delta x^+, \Delta z^+$ values are usually well below 50. Even though some regions go beyond 60, they are known to be laminar regions. Moreover, y^+ values being lower than six are also acceptable with $p = 3$ in mind, because the first solution point over the wall is below $y^+ = 1$. This is rather conservative for $p = 3$, as found by Drosson et al. (2013).
Figure 12a compares isentropic Mach number distribution on the blade with the reference data. Although the smooth case results are consistent with the reference DNS results (Hillewaert et al., 2014), the experimental measurements (Michálek et al., 2012) show otherwise. In fact, this was also observed in numerous studies, leading to the conclusion that the conditions of the experiment are actually different (Hillewaert et al., 2014, 2016; Alhawwary and Wang, 2019; Bergmann et al., 2021). Among others, some of the differences are the lack of turbulence at the inlet and a possible discrepancy in the inflow angle. Regardless, the results from the experiment are also included for completeness. The rough case shows only a slight deviation around the separation region ($x/c_{\mathrm{ax}} \approx 0.70$), indicating that the roughness patch is not rough enough. The same observation can be made for the skin friction plot (Figure 12b). The location of the separation point ($c_f \approx 0$) moves downstream only a bit. A slightly earlier transition to turbulence $x/c_{\mathrm{ax}} \approx 0.95$ can also be observed. In fact, an investigation with a rougher surface would be more interesting.
Figure 13 compares the total pressure loss in the wake at $0.465 c_{\mathrm{ax}}$ aft of the trailing edge. The loss is calculated as,

$$\zeta(y) = 1 - \frac{\overline{p_0(y,t)}}{\overline{p_{0,\mathrm{inlet}}(t)}} \tag{2}$$

where $\overline{p_{0,\mathrm{inlet}}(t)}$ is taken as the enforced boundary condition. It should be noted that the relative location of the wake in the experiment is arbitrary because the frame of reference is not known. Hence, the wake profiles of the smooth cases are shifted towards the Bergmann et al. (2021) results so that the peak locations meet. The wake is known to be drastically influenced by the

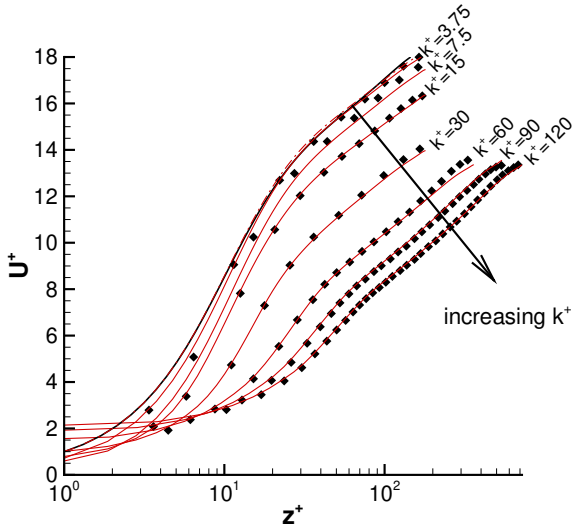

Fig. 6: Mean velocity profiles in wall units. Black points represent DNS by Thakkar et al. (2018); red solid lines are current results, 1, 2, 3, 4d, 5, 6, 7; dashdotted line is the current smooth reference; black solid line is the smooth reference DNS with $\mathrm{Re}_\tau \approx 180$ (Lee and Moser, 2015)

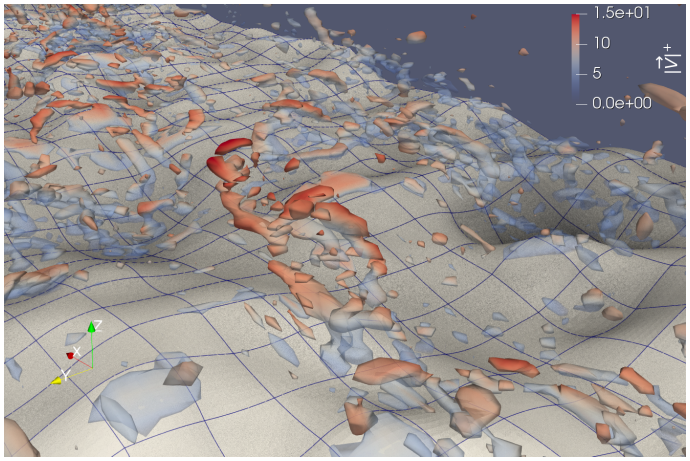

Fig. 7: Isosurface of Q-criterion for $Re_\tau = 720$ (Sim. 7) coloured by the velocity magnitude in wall units. The surface mesh is also shown.

boundary layer and the turbulence state over the blade. The peak loss from the experiment looks totally different, probably for the same reason as the M_s distribution. There is a relatively good agreement on peaks between the LES by Bergmann et al. (2021) and our smooth solution. The roughness causes a narrower wake as well as a slight diminishing of the peak, owing to the fact that the roughness shrinks the separation bubble. The loss peak also moves slightly towards the PS due to the roughness-related wake deflection.

A set of measurement points are placed in the wake $0.465c_{ax}$ downstream the trailing edge as shown Figure 14. The turbulence spectra on the wake probes are shown in Figure 15. The roughness has indeed some effect on the flow. The energy peak related with the separation bubble at around $fc/U_{out} \approx 2$ cannot be observed in the rough case. Moreover, a decrease in overall turbulence energy on point 4 can be observed.

4 Conclusion and Outlook

A novel approach to predicting the impact of roughness on the boundary layer and the wake is proposed. In the rough channel setup, the method proves to be competitive compared to IBM. It not only yields high accuracy, but also allows LES without sacrificing the topological features of the filtered rough surface. Above all, efficient simulation of slightly rough surfaces, ranging from hydraulically smooth to the transitionally rough regime ($0 < k_s^+ < 70$), is made possible. In this roughness range, other methods like the IBM can fall into over-resolved DNS if the roughness is to be preserved well. In contrast, in the present method, LES-level resolutions are shown to be adequate for resolving the surface sufficiently.

Moreover, based on North-German Supercomputing Alliance's pricing policy, the method proposed hints at reduced expenses. When the validation case $Re_\tau = 180$ ($p = 3$) is run on V100 GPUs with a comparable mesh resolution, the method saves up to 75% compared with the DNS with second-order finite volume method run on CPU's by Kurth et al. (2021). Indeed, this amount of

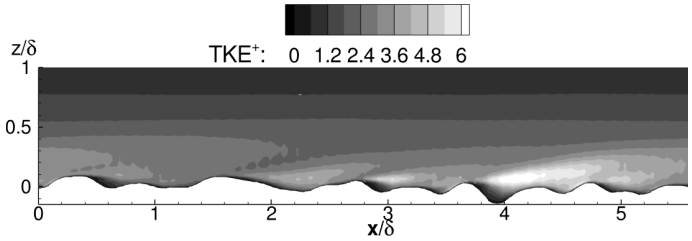

Fig. 8: Turbulent kinetic energy for $Re_\tau = 720$ (Sim. 7) in wall units, taken from the mid-span plane.

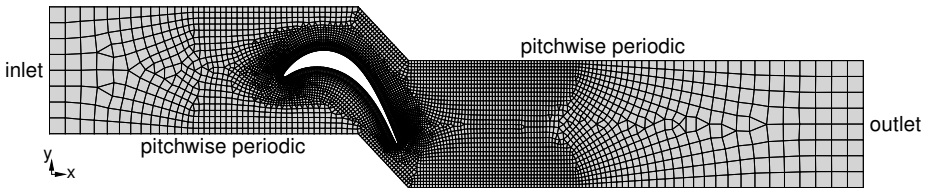

Fig. 9: The computational domain

financial cost reduction is found be quite promising.

The method is also applied to the case of a low-pressure turbine (LPT) cascade with and without a roughness patch on the suction side of the profile. ILES of the smooth blade provide accurate results. The rough blade however, turns out not to be rough enough, such that it does not have a clearly discernible impact on the isentropic Mach number and skin friction distributions. However, the roughness does have some effect on the wake total pressure loss and wake turbulence spectra, particularly on the suction side of the wake.

The future work will cover the influence of roughness on the aerodynamic performance of compressor and turbine cascades. Based on this, available roughness models for industrial applications will be assessed.

Acknowledgment and Funding Information

This research did not receive any specific grant from funding agencies in the public, commercial, or non-for-profit sectors.

The computational resources were was partially provided by the North-German Supercomputing Alliance (HLRN) and partially by the cluster system team at the Leibniz University of Hannover (LUIS), Germany. We gratefully appreciate the provided resources.

References

Mohammad Alhawwary and Z. J. Wang. On the mesh resolution of industrial les based on the dns of flow over the T106C turbine. *Advances in Aerodynamics*, 1(1):21, Dec 2019. doi: 10.1186/s42774-019-0023-6.

Michael Bergmann, Christian Morsbach, Graham Ashcroft, and Edmund Kügeler. Statistical error estimation methods for engineering-relevant quantities from scale-resolving simulations. *Journal of Turbomachinery*, 144(3), 10 2021. doi: 10.1115/1.4052402.

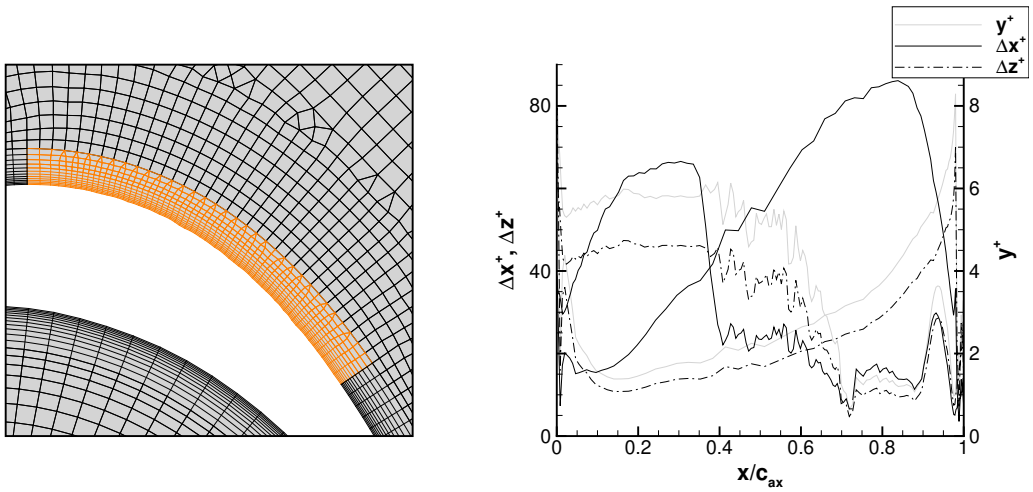

Fig. 10: a) The roughness block, highlighted with orange, b) the elemental resolution on the blade in streamwise, spanwise, and wall-normal directions ($\Delta x^+, \Delta z^+, y^+$)

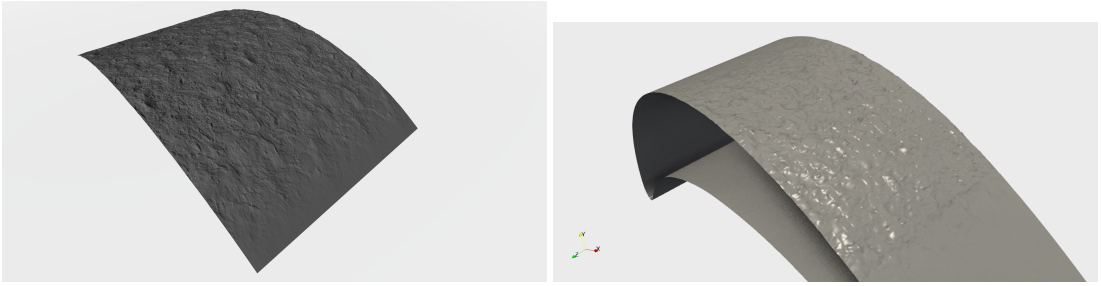

Fig. 11: The original roughness patch placed on the blade section (left), the roughness on the blade as perceived by the mesh (right)

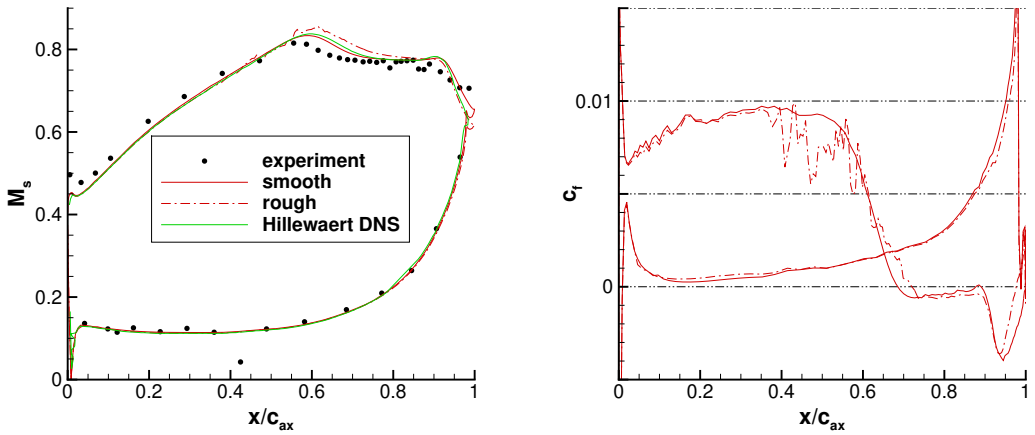

Fig. 12: isentropic Mach distribution (left), and skin-friction coefficient distribution over the blade

Angela Busse, Mark Lützner, and Neil D. Sandham. Direct numerical simulation of turbulent flow over a rough surface based on a surface scan. *Computers & Fluids*, 116:129–147, 2015. doi: 10.1016/j.compfluid.2015.04.008.

Daniel Chung, Nicholas Hutchins, Michael P. Schultz, and Karen A. Flack. Predicting the drag of rough surfaces. *Annual Review of Fluid Mechanics*, 53(1):439–471, 2021. doi: 10.1146/annurev-fluid-062520-115127.

Marie Denison, Anirban Garai, and Scott Murman. Preliminary scale-resolving simulations of laminar-to-turbulent transition in swept-wing flow. In *AIAA Aviation 2019 Forum*, page 3534, 2019. doi: 10.2514/6.2019-3534.

DIN EN ISO 25178-2. Geometrische Produktspezifikation (GPS) - Oberflächen-beschaffenheit: Flächenhaft - Teil 2: Begriffe und Oberflächen-Kenngrößen (ISO 25178-2:2012), Deutsche Fassung EN ISO 25178-2:2012. *Beuth Verlag*, 2012.

Laslo T Diosady and Scott M Murman. A linear-elasticity solver for higher-order space-time mesh deformation. In *AIAA Aerospace Sciences Meeting*, page 0919, 2018. doi: 10.2514/6.2018-0919.

R.B. Dirling. A method for computing roughwall heat transfer rates on reentry nosetips. In *8th Thermophysics Conference*, page 763, 1973. doi: 10.2514/6.1973-763.

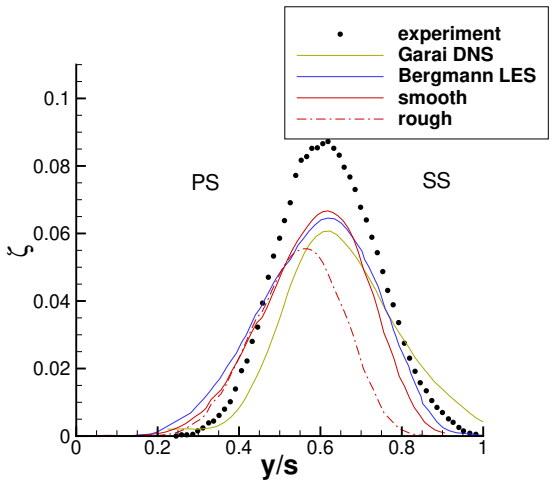

Fig. 13: Total pressure loss in the wake $0.465c_{ax}$ aft of the trailing edge (Garai et al., 2016; Bergmann et al., 2021; Michálek et al., 2012)

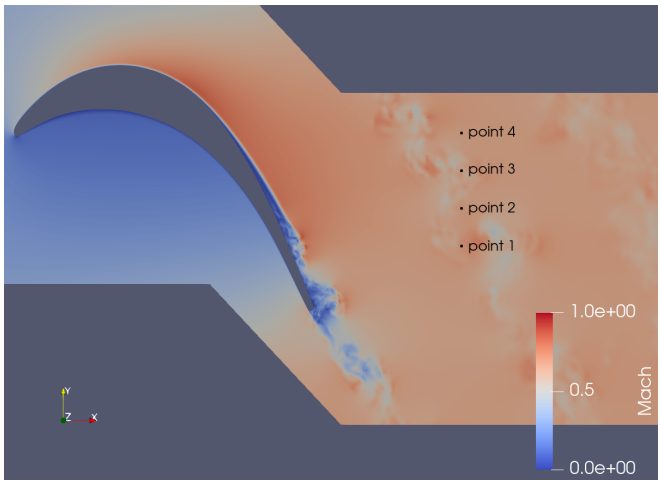

Fig. 14: Rough blade instantaneous Mach number distribution and the location of the probes in the wake

DLR. 2nd international workshop on high-order cfd methods, 2013. URL https://www.dlr.de/as/desktopdefault.aspx/tabid-8170/28275_read-35550/. [Online; accessed 7th March 2022].

Marcus Drosson, Koen Hillewaert, and Jean-André Essers. Stability and boundary resolution analysis of the discontinuous galerkin method applied to the reynolds-averaged navier–stokes equations using the spalart–allmaras model. *SIAM Journal on Scientific Computing*, 35(3):B666–B700, 2013. doi: 10.1137/110834615.

Anirban Garai, Laslo T. Diosady, Scott M. Murman, and Nateri K. Madavan. DNS of low-pressure turbine cascade flows with elevated inflow turbulence using a discontinuous-galerkin spectral-element method. In *Turbo Expo: Power for Land, Sea, and Air*, volume Volume 2C: Turbomachinery. American Society of Mechanical Engineers, 06 2016. doi: 10.1115/GT2016-56700.

Anirban Garai, Laslo T. Diosady, Scott M. Murman, and Nateri K. Madavan. Scale-resolving simulations of low-pressure turbine cascades with wall roughness using a spectral-element method. In *Turbo Expo: Power for Land, Sea, and Air*, volume Volume 2C: Turbomachinery. American Society of Mechanical Engineers, 06 2018. doi: 10.1115/GT2018-75982.

F. Hammer, Neil D. Sandham, and Richard D. Sandberg. Large eddy simulations of a low-pressure turbine: Roughness modeling and the effects on boundary layer transition and losses. In *Turbo Expo: Power for Land, Sea, and Air*, volume Volume 2B: Turbomachinery. American Society of Mechanical Engineers, June 2018. doi: 10.1115/GT2018-75796.

Konrad M Hartung, Philipp Gilge, and Florian Herbst. Towards immersed boundary methods for complex roughness structures in scale-resolving simulations. In *ECMS*, pages 359–365, 2018. doi: 10.7148/2018-0359.

K Hillewaert, R Hartmann, T Leicht, V Couaillier, ZJ Wang, and JS Cagnone. Summary and conclusions of the 4th international workshop on high order cfd methods. *ECCOMAS. Crete, Greece*, 2016.

Koen Hillewaert, Corentin Carton de Wiart, Guillaume Verheylewegen, and Tony Arts. Assessment of a high-order discontinuous galerkin method for the direct numerical simulation of transition at low-reynolds number in the T106C high-lift low pressure turbine cascade. In *Turbo Expo: Power for Land, Sea, and Air*, volume Volume 2B: Turbomachinery. American Society of Mechanical Engineers, 06 2014. doi: 10.1115/GT2014-26739.

F. Hindenlang, T. Bolemann, and C. D. Munz. *Mesh Curving Techniques for High Order Discontinuous Galerkin Simulations*, pages 133–152. Springer International Publishing, 2015. doi: 10.1007/978-3-319-12886-3_8.

Jongwook Joo, Gorazd Medic, and Om Sharma. Large-Eddy Simulation Investigation of Impact of Roughness on Flow in a Low-Pressure Turbine. In *Turbo Expo: Power for Land, Sea, and Air*, volume Volume 2C: Turbomachinery of *Turbo Expo: Power for Land, Sea, and Air*, 06 2016. doi: 10.1115/GT2016-57912.

Steve L Karman, J T Erwin, Ryan S Glasby, and Douglas Stefanski. High-order mesh curving using WCN mesh optimization. In *46th AIAA Fluid Dynamics Conference*, page 3178, 2016. doi: 10.2514/6.2016-3178.

Nico Krais, Andrea Beck, Thomas Bolemann, Hannes Frank, David Flad, Gregor Gassner, Florian Hindenlang, Malte Hoffmann, Thomas Kuhn, Matthias Sonntag, and Claus-Dieter Munz. Flexi: A high order discontinuous galerkin framework for hyperbolic–parabolic conservation laws. *Computers & Mathematics with Applications*, 81:186–219, 2021. doi: 10.1016/j.camwa.2020.05.004. Development and Application of Open-source Software for Problems with Numerical PDEs.

Sebastian Kurth, Kenan Cengiz, Lars Wein, and Joerg R. Seume. From measurement to simulation: A review of aerodynamic investigations of real rough surfaces by DNS. In *Proceedings of the Global Power and Propulsion Society (GPPS)*, page 213, October 2021. doi: 10.33737/gpps21-tc-213.

Myoungkyu Lee and Robert D. Moser. Direct numerical simulation of turbulent channel flow up to $Re_\tau \approx 5200$. *Journal of Fluid Mechanics*, 774:395–415, 2015. doi: 10.1017/jfm.2015.268.

S. Leonardi, P. Orlandi, and R. A. Antonia. Properties of d- and k-type roughness in a turbulent channel flow. *Physics of Fluids*, 19 (12):125101, 2007. doi: 10.1063/1.2821908.

R. Mejia-Alvarez and K. T. Christensen. Low-order representations of irregular surface roughness and their impact on a turbulent boundary layer. *Physics of Fluids*, 22(1):015106, 2010. doi: 10.1063/1.3291076.

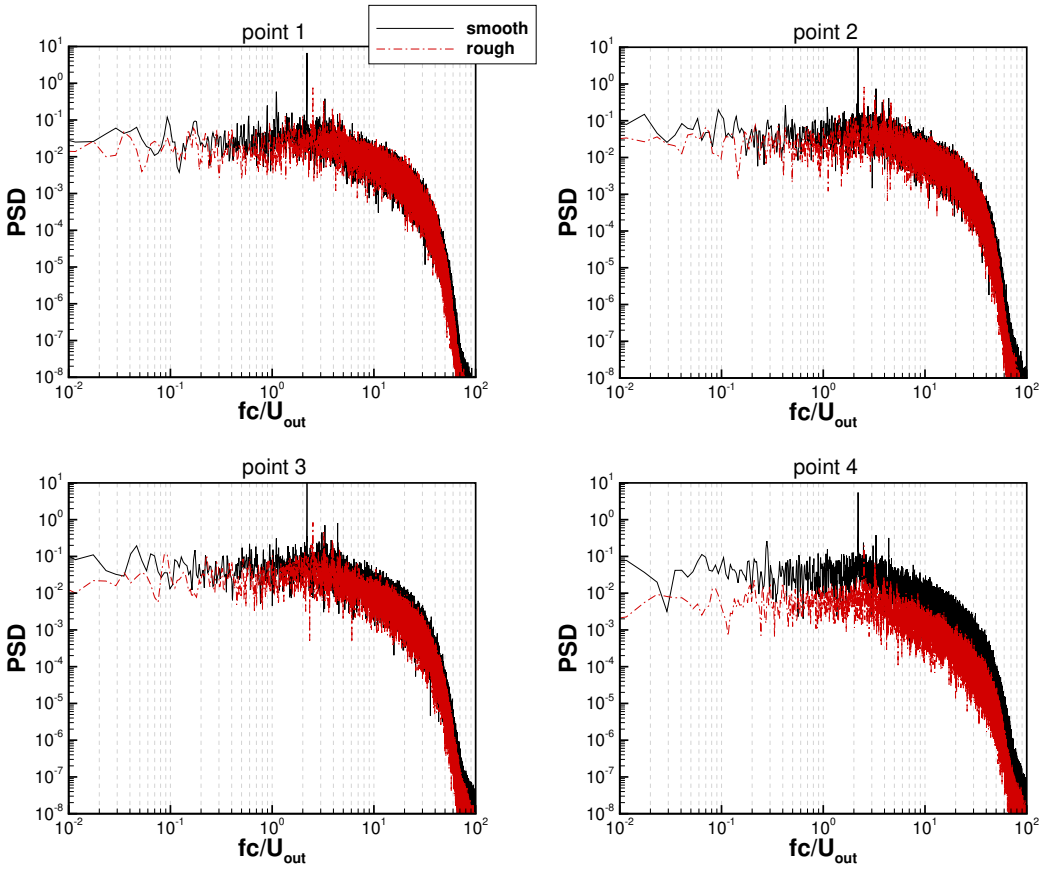

Fig. 15: Turbulence power spectral density on points 1–4

Jan Michálek, Michelangelo Monaldi, and Tony Arts. Aerodynamic Performance of a Very High Lift Low Pressure Turbine Airfoil (T106C) at Low Reynolds and High Mach Number With Effect of Free Stream Turbulence Intensity. *Journal of Turbomachinery*, 134(6), 08 2012. doi: 10.1115/1.4006291. 061009.

Stephen K. Roberts and Metin I. Yaras. Effects of Surface-Roughness Geometry on Separation-Bubble Transition. *Journal of Turbomachinery*, 128(2):349–356, 02 2005. doi: 10.1115/1.2101852.

Asher Sigal and James E. Danberg. New correlation of roughness density effect on the turbulent boundary layer. *AIAA Journal*, 28 (3):554–556, 1990. doi: 10.2514/3.10427.

M. Thakkar, A. Busse, and N. D. Sandham. Direct numerical simulation of turbulent channel flow over a surrogate for nikuradse-type roughness. *Journal of Fluid Mechanics*, 837:R1, 2018. doi: 10.1017/jfm.2017.873.

Manan Thakkar, Angela Busse, and Neil Sandham. Surface correlations of hydrodynamic drag for transitionally rough engineering surfaces. *Journal of Turbulence*, 18(2):138–169, 2017. doi: 10.1080/14685248.2016.1258119.

Nagabhushana Rao Vadlamani, Paul G Tucker, and Paul Durbin. Distributed roughness effects on transitional and turbulent boundary layers. *Flow, Turbulence and Combustion*, 100:627–649, 2018. doi: 10.1007/s10494-017-9864-4.

F. D. Witherden and A. Jameson. Impact of number representation for high-order implicit large-eddy simulations. *AIAA Journal*, 58(1):184–197, 2020. doi: 10.2514/1.J058434.

F.D. Witherden, A.M. Farrington, and P.E. Vincent. Pyfr: An open source framework for solving advection–diffusion type problems on streaming architectures using the flux reconstruction approach. *Computer Physics Communications*, 185(11): 3028–3040, 2014. doi: 10.1016/j.cpc.2014.07.011.